



This is a repository copy of *Quantum dot superluminescent diodes for optical coherence tomography: device engineering*.

White Rose Research Online URL for this paper:
<http://eprints.whiterose.ac.uk/42656/>

Article:

Greenwood, P.D.L., Childs, D.T.D., Kennedy, K. et al. (10 more authors) (2010) Quantum dot superluminescent diodes for optical coherence tomography: device engineering. *IEEE Journal of Selected Topics in Quantum Electronics*, 16 (4). pp. 1015-1022. ISSN 1077-260X

<https://doi.org/10.1109/JSTQE.2009.2038720>

Reuse

Unless indicated otherwise, fulltext items are protected by copyright with all rights reserved. The copyright exception in section 29 of the Copyright, Designs and Patents Act 1988 allows the making of a single copy solely for the purpose of non-commercial research or private study within the limits of fair dealing. The publisher or other rights-holder may allow further reproduction and re-use of this version - refer to the White Rose Research Online record for this item. Where records identify the publisher as the copyright holder, users can verify any specific terms of use on the publisher's website.

Takedown

If you consider content in White Rose Research Online to be in breach of UK law, please notify us by emailing eprints@whiterose.ac.uk including the URL of the record and the reason for the withdrawal request.



eprints@whiterose.ac.uk
<https://eprints.whiterose.ac.uk/>

Quantum Dot Superluminescent Diodes for Optical Coherence Tomography: Device Engineering

Purnima D. L. Greenwood, David T. D. Childs, Kenneth Kennedy, Kristian M. Groom, Maxime Hugues, Mark Hopkinson, Richard A. Hogg, Nikola Krstajić, Louise E. Smith, Stephen J. Matcher, Marco Bonesi, Sheila MacNeil, and Rod Smallwood

Abstract—We present a 18 mW fiber-coupled single-mode superluminescent diode with 85 nm bandwidth for application in optical coherence tomography (OCT). First, we describe the effect of quantum dot (QD) growth temperature on optical spectrum and gain, highlighting the need for the optimization of epitaxy for broadband applications. Then, by incorporating this improved material into a multicontact device, we show how bandwidth and power can be controlled. We then go on to show how the spectral shape influences the autocorrelation function, which exhibits a coherence length of $<11 \mu\text{m}$, and relative noise is found to be 10 dB lower than that of a thermal source. Finally, we apply the optimum device to OCT of *in vivo* skin and show the improvement that can be made with higher power, wider bandwidth, and lower noise, respectively.

Index Terms—Optical coherence tomography (OCT), quantum dot (QD), skin imaging, superluminescent diodes (SLEDs).

I. INTRODUCTION

OPTICAL coherence tomography (OCT) utilizes low coherence interferometry to image the near surface of biological specimens. The simplest embodiment of this imaging technique, time-domain OCT (TD OCT) utilizes broadband radiation injected into an interferometer, where the two arms are composed of a translating reference mirror and a biological specimen. The interference signal arises from the light reflected from the specimen at a depth determined by the path length in the reference arm. By changing this path length in time, different depths of tissue can be interrogated, which, combined with rastering the beam, allows a full 3-D image to be created. For OCT systems, a broadband light source is required, since axial resolution is governed by the coherence length. In the laboratory, ultrafast mode-locked laser systems can be used to create broadband light [1], [2], while for lower cost and robust clinical applications a superluminescent diode (SLED) is used. Fourier domain variants of OCT are of increasing interest due to a significant increase in SNR [3], [4], and offer the prospect of high-resolution video rate imaging [5]. Spectral/Fourier-domain

OCT systems [6] also utilize broadband sources with identical requirements as TD OCT, i.e., high spectral bandwidth, high single-mode fiber-coupled power, low noise, low cost, and ease of use. Key wavelengths for OCT sources are typically 1050 nm for ophthalmology (minimum of optical dispersion in water) [7] and $\sim 1200\text{--}1300$ nm for imaging skin tissue (minimum in scattering and absorption) [8].

Recently, self-assembled quantum dots (QDs) have attracted interest as the active element in SLEDs [9], [10]. QDs offer the advantage of inhomogeneously broadened states, which may be readily saturated to employ both ground and excited states in the emission spectrum [9], [10]. QD SLEDs are typically operated at a current where the emission from two of the QD states balances, for example, where the power from the ground state and first excited state is balanced by providing a maximum in emission linewidth and corresponding minimum in coherence length, so maximizing resolution. For QD SLEDs, the emission power, device length, spectral shape, and bandwidth are interlinked [11], and a spectral dip is usual [12]. A multicontact device structure has been developed by us, allowing the spectral shape, and so the point spread function (PSF) of the interferometer to be tuned [13]. The spectral dip, undesirable for OCT due to the possibility of ghost images [14], is typically reduced by varying the emission wavelength of individual QD layers in a multilayer stack [15]. However, this technique wastes optical gain, which tends to reduce overall device efficiency, since the first excited state of short wavelength QDs overlaps with the strongly absorbing second excited state of the long-wavelength QDs. Carriers in these QD states may not efficiently contribute to the output spectrum.

In this paper, we present latest device results for broadband high-power QD SLED for OCT applications. Epitaxial methods for reducing the spectral dip are discussed, and the configuration of a multicontact device utilizing this material is detailed. A comparison of the noise characteristics of this device with a commercial quantum well (QW) SLED is made, and the effects of increased power, reduced noise, and increased bandwidth on TD OCT imaging is presented.

II. BANDWIDTH ENGINEERING IN QD DEVICES

The optimization of epitaxial growth of QD materials requires high QD aerial density (realizing high-gain and spontaneous emission), high inhomogeneity (yielding an inhomogeneous broadening greater than the ground and excited state splitting), along with low-defect density (ensuring nonradiative recombination is minimized). As the output power spectrum

Manuscript received August 5, 2009; revised September 30, 2009; accepted December 6, 2009. Date of publication April 8, 2010; date of current version August 6, 2010. This work was supported by the United Kingdom Biotechnology and Biological Sciences Research Council under Grant BB/E002676/1.

P. D. L. Greenwood, D. T. D. Childs, K. Kennedy, K. M. Groom, M. Hugues, M. Hopkinson, and R. A. Hogg are with the Department of Electronic and Electrical Engineering, University of Sheffield, Sheffield, S1 3JD, U.K. (e-mail: elp05pdj@sheffield.ac.uk; r.hogg@sheffield.ac.uk).

N. Krstajić and R. Smallwood are with the Department of Computer Science, University of Sheffield, Sheffield, S1 3JD, U.K.

L. E. Smith, S. J. Matcher, and S. MacNeil are with the Department of Engineering Materials, University of Sheffield, Sheffield, S1 3JD, U.K.

M. Bonesi is with the Medical University of Vienna, Vienna, Austria.

Digital Object Identifier 10.1109/JSTQE.2009.2038720

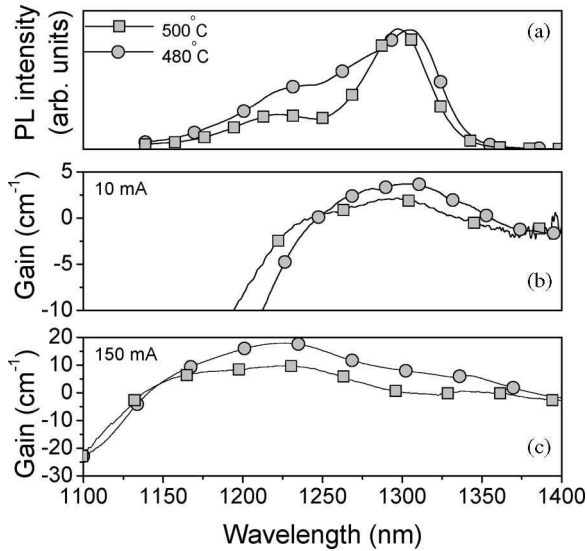


Fig. 1. (a) Photoluminescence and (b), (c) gain spectra of QD laser material at two different growth temperatures for the QD layers, at room temperature.

is linear with regard to spontaneous emission, yet exponential with optical gain, it follows that gain spectrum measurements are crucial in optimizing the epitaxial growth of QD SLED material. For epitaxy optimization studies, a series of samples was grown, where key parameters were varied. Nondestructive material characterization, gain spectra measurements, and SLED device characteristics were all compared for various growth parameters. Seven InAs/InGaAs dot-in-a-well [16] layers separated by 50 nm of GaAs formed the active region of the QD SLED. Waveguiding was provided by doped $\text{Al}_{0.4}\text{Ga}_{0.6}\text{As}$ cladding layers. The details of the epitaxial growth can be found in previous reports on QD laser epitaxy development [17].

Fig. 1(a) shows photoluminescence (PL) spectra obtained with identical experimental conditions, and continuous wave (CW) gain spectra at 10 and 150 mA, respectively, of two wafers grown sequentially in a growth campaign [see Fig. 1(b) and (c)]. For these two samples, only the deposition temperature of the QD layers and low-temperature GaAs cap was changed. The usual deposition temperature for QD laser material is 500 °C. PL spectra for the 500 °C sample exhibit well-resolved ground state (1300 nm) and excited state (1220 nm) emission with both states having a linewidth ~ 50 nm. Reduction in the temperature of QD deposition to 480 °C results in a number of significant changes. The QD states become less well resolved, with a broadening to higher energies of the ground-state peak. The gain spectrum for the 500 °C sample obtained by the variable stripe length technique [18] at 10 mA also exhibits a peak at this wavelength, corresponding to the ground state of the QD ensemble. The strong reduction in gain and onset of absorption at short wavelengths is due to the second excited state, which is not significantly populated at these carrier densities. At higher carrier densities [see Fig. 1(c)], the gain peak is shifted to ~ 1220 nm, corresponding to the excited state of the QDs. At a current of 20 mA the gain from excited and ground state is roughly balanced. The 3 dB gain bandwidths for the sample grown at

500 °C are 120 and 50 nm, at 10 and 150 mA, respectively. For the sample grown at 480 °C, the 3 dB gain bandwidths are 120 and 55 nm at 10 and 150 mA, respectively.

The longitudinal multiplexing of two devices operated under drive conditions close to these two current densities is found to be optimal in achieving a broad high-power emission with low spectral dip. The internal losses of these two devices (in the limit of long wavelength) are essentially identical at 2 cm^{-1} . The increase in the peak gain, at all applied currents is also of key importance. This may be attributed to an increased nonradiative carrier lifetime and/or an increased QD density.

The size and composition of QDs are strong functions of the growth temperature, leading to changes in the emission energy and spectral width. As the growth temperature is reduced, the indium surface migration length is reduced, acting to reduce the dot size and increase the dot density [19] through a mechanism, which favors accumulation at increasingly localized sites. These structural changes induce a blue shift in the emission energy [20], but this may be partially offset by an increase in indium incorporation at the growth front at the lower growth temperature. A widening of the inhomogeneous distribution, which we exploit in this application is also associated with a reduction in growth temperature. A major effect of lowering the growth temperature in the reduced indium migration length results in a less uniform ensemble of QDs, and can give rise to distinctly different QD distributions within the same sample. Indeed, bi and multimodal size distributions are commonly seen at low growth temperatures [21], [22]. Controlled overlap of these sub-distributions within the whole ensemble of QDs can result in a further broadening of the emission and gain spectrum. Therefore the broadening of the ground state ensemble and the filling of the gap between the ground and the excited state energies is necessary for optimum device performance.

III. DEVICE DESIGN AND FABRICATION

We utilize a multicontact device that allows the separation of the link between output power and emission spectrum shape [23], [24]. While a dual-pass device with antireflection/high-reflection facets allows high powers, the single-pass device presented here renders the device less sensitive to external feedback. High feedback causes lasing from the SLED, merely rendering OCT imaging impossible, rather than physically damaging the device [25].

Fig. 2(a) shows a schematic of our device. It consists of a 9 mm long, $7\ \mu\text{m}$ wide ridge with 1 mm isolated contact sections. At the rear of the device is a ~ 1 mm long, $300\ \mu\text{m}$ wide tapered absorber section with a tilted, deep v-etched back facet, to eliminate reflections [26]. The absorber section was unbiased for this work, but could also be used to apply a reverse voltage while driving the device. The output facet of the device is at a 7° angle due to a bend (radius of curvature 1.625 cm) of the waveguide. The length of the curved waveguide is chosen to be 2 mm because it offers a compromise between minimum waveguide loss and minimum chip real estate.

The devices were patterned using vacuum contact lithography and trenches made by inductively coupled plasma etching

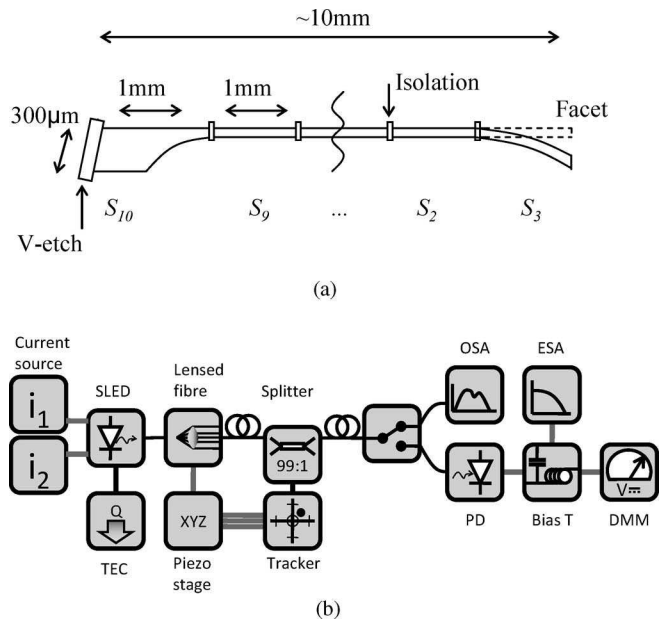


Fig. 2. (a) Schematic of fabricated device structure. (b). Schematic of the SLED setup for optical and electrical measurements.

of the waveguide to a depth of $2.0 \mu\text{m}$ (i.e., stopping above the active region core) via a double trench, using a silicon tetrachloride-based etch. Each 1 mm section was electrically isolated by means of a $50 \mu\text{m}$ long shallow etch of the GaAs p^+ contact layer, providing a resistance of $\sim 2 \text{ k}\Omega$ between adjacent contacts. Evaporated Au–Zn–Au top contacts followed by electroplated bond-pads were then applied. The current–voltage characteristics of individual sections of a given device are essentially identical, which greatly simplifies the driving circuitry when multiple sections are driven together [27].

IV. DEVICE CHARACTERISTICS

Fig. 3(a) shows the electroluminescence spectra for a SLED device, fabricated from the $480 \text{ }^\circ\text{C}$ sample with various drive currents applied to the front nine sections (the rear absorber section was left open circuit). The solid line corresponding to 153 mA, supplied to each of the front three sections and 11 mA in sections four to nine, produces the broadest, flattest emission spectrum with $\sim 18 \text{ mW}$ of power coupled into the single-mode fiber. A spectral modulation of $\sim 0.87 \text{ dB}$ is measured. Reducing (increasing) the currents results in a reduction (increase) in the optical power along with a dominance of the spectrum by the QD ground states (excited states). In order to simplify the drive electronics, sections one to three were connected and driven with a single current source, while sections four to nine were similarly shorted and connected to another current source. The ratio of currents was chosen to duplicate that of the solid line in Fig. 3(a) (460:70). Fig. 3(b) shows the optical power as a function of total drive current of the device driven, maintaining constant ratio. The inset shows the emission spectrum of the device at each of the data points. Further simplification of the drive circuitry is possible by the implementation of a resistor network to realize the use of a single current source [27].

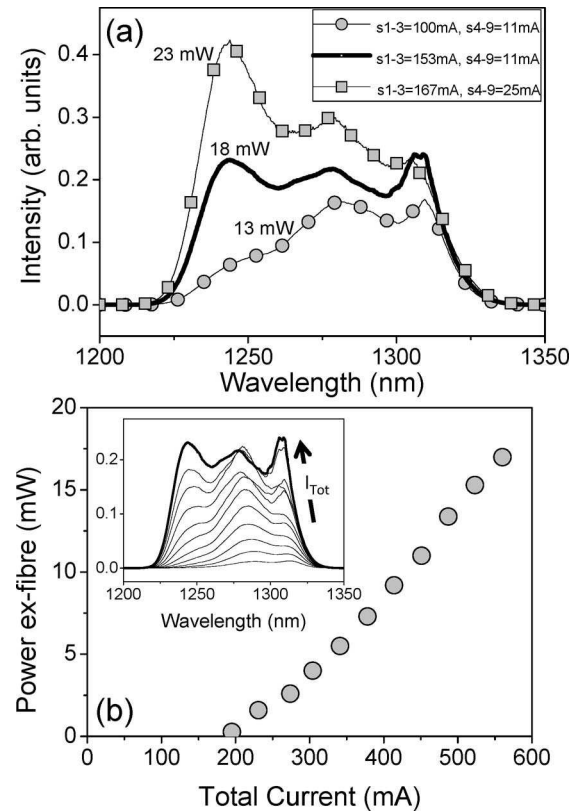


Fig. 3. (a) Emission spectrum as a function of different drive configurations (see Fig. 2) for the QD SLED. (b) Total ex-fiber optical power to maintain a current ratio equal to that of the solid line in (a). Inset shows emission spectrum as a function of increasing total current. All measurements were carried out in CW operation.

For application in OCT systems, the spectral shape is significant due to pixel formation being essentially a Fourier transform process in the interferometer. The detected signal from a single-reflection plane for low-coherence imaging is given by the self-coherence function. This function is given by the inverse Fourier transform of the power spectral density of the source and can be regarded as the PSF of the imaging system [13]. Fig. 4(a) shows the PSF, calculated from the emission spectra shown in the inset of Fig. 3(b). Good correlation between calculated and measured PSFs has been found [28]. The side-lobe suppression ratio and 3 dB linewidth of the device are plotted in Fig. 4(b). A high side-lobe suppression ratio indicates smaller optical powers in different frequency components of the optical spectrum, and indicates lower noise and reduced strength of ghost images. A small 3 dB linewidth indicates increased axial resolution.

As total current is increased, so the side-lobe suppression ratio increases from $\sim 10 \text{ dB}$ (total current = 200 mA, ex-fiber optical power = 1 mW) to 12 dB (total current = 350 mA, ex-fiber optical power = 6 mW). Subsequently as total current is increased, the side-lobe suppression ratio reduces to 7.5 dB at 550 mA (ex-fiber optical power = 23 mW). The 3 dB linewidth is observed to decrease monotonically with total current, reaching $11 \mu\text{m}$ at currents $> 450 \text{ mA}$, indicating an increase in resolution with increasing current. There is therefore a trade off when deciding the device current with increased side-lobe power as

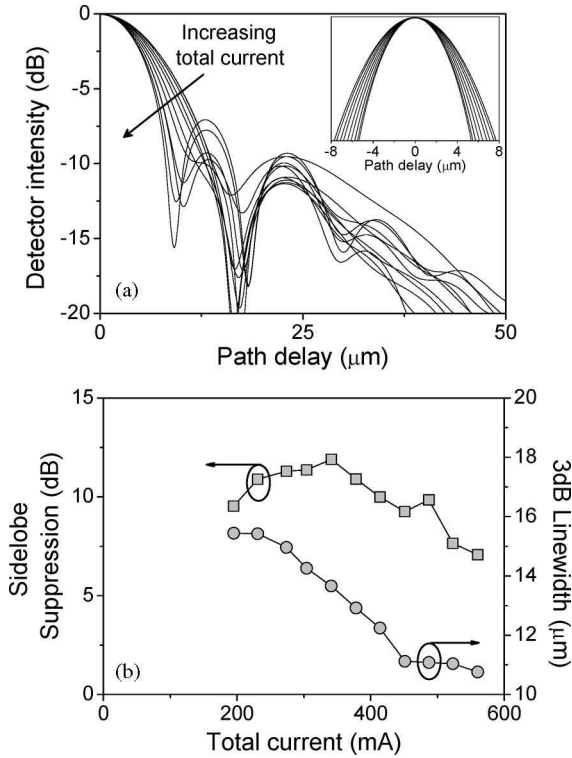


Fig. 4. (a) Autocorrelation function of the emission spectra shown in the inset of Fig. 3(b). Inset shows expanded scale around zero path length. (b) Sidelobe suppression ratio and 3 dB bandwidth determined from the autocorrelation function.

power is increased in the region where total current = 450 mA to 550 mA.

V. COMPARISON WITH A LOWER BANDWIDTH DEVICE

A commercial QW SLED was used to provide this comparison to our QD SLED. A Superlum Ltd. 561-MP device was used, which has a lower emission power (~1 mW compared to ~20 mW) and lower bandwidth (~45 nm compared to ~85 nm) than the QD SLED described here. While a comparison of the devices is clouded by these differences in output rather than the physical differences between QWs and QDs, some comparison is still meaningful namely the operation of the QD SLED in gain saturation that impacts upon spectral width and the relative intensity noise (RIN). Additionally, the effects of these device specification differences upon TD OCT image quality are also instructive.

Measuring optical spectra as a function of emission power for the QW SLED (see inset of Fig. 5) allows a plot of emission linewidth as a function of power to be made, which is shown in Fig. 5. The reduction of linewidth is characteristic of an SLED, which exhibits an increase in peak gain with increasing current, reducing the emission linewidth. In QD SLEDs, operated in a condition of gain saturation, the bandwidth can be made to increase with increasing current. The shift to shorter wavelengths is consistent with band filling in the QWs. It should be noted that broader emission is possible from QW devices

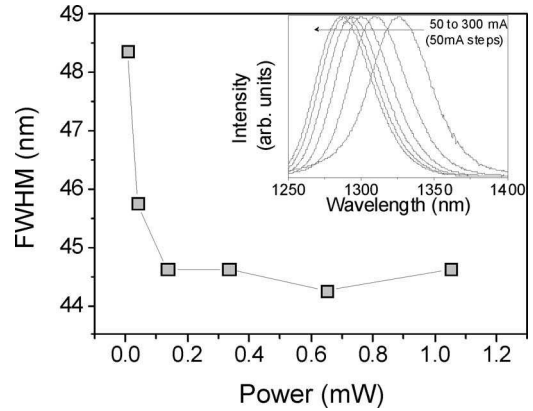


Fig. 5. Full-width at half-maximum as a function of emission power for a commercial QW SLED. Inset shows normalized emission spectrum as a function of drive current.

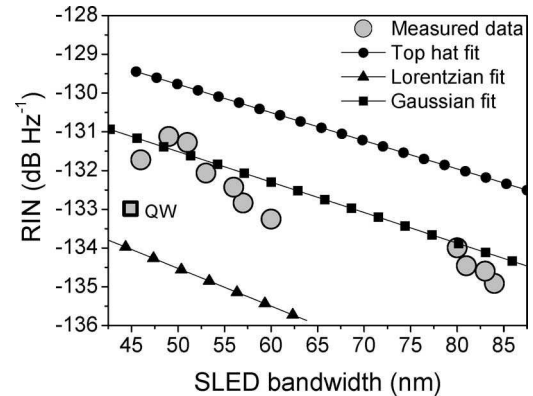


Fig. 6. White noise background as a function of QD SLED bandwidth. The black line with square symbols represents the expected values assuming a thermal noise source, for a Gaussian fit, while the triangles and circles represent Lorentzian and top hat fits, respectively. The value for the QW SLED at 1 mW output power is also plotted.

using, for example, asymmetric double QWs, which rely upon thermalization of carriers between the wells.

Another key factor in OCT image quality is the signal to noise ratio (SNR). This is determined by the detection bandwidth and RIN spectrum of the optical source. The noise of the optical sources was measured in the electrical frequency domain by an Agilent E4440A electrical spectrum analyzer, via an Agilent 11982A lightwave converter, as shown in Fig. 2(b). High output powers from the device under test are attenuated down to 1 mW by a neutral density optical filter at the photodiode, to prevent saturation. The electrical output of the optical to electrical converter is fed into an electrical spectrum analyzer. In order to convert noise spectral density to RIN, the dc power level is measured using a Keithley 2000 multimeter via a 50-Ω termination resistor.

Fig. 6 plots the noise background of the QD SLED source as a function of emission bandwidth. The 3 dB bandwidth of a noise spectrum is approximately equal to the source linewidth for a thermal source, such as this device where the light generation occurs via random spontaneous emission. Since an optical bandwidth of 1 nm results in over 180 GHz of electrical noise

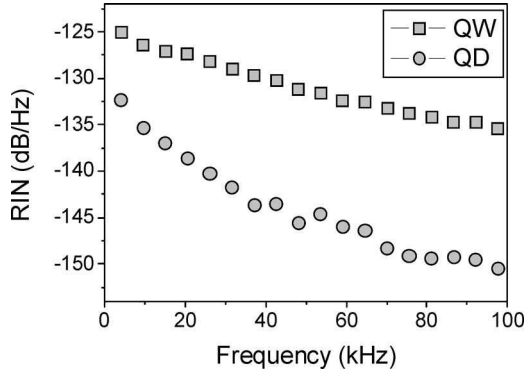


Fig. 7. Low-frequency RIN spectra for QD (17 mW, 85-nm bandwidth) and QW (1 mW, 45-nm bandwidth) devices.

bandwidth, this can be considered as a pure white noise source for all practical detection frequencies. Fits are also shown for a “top hat” and a Lorentzian shape. The difference in Gaussian to “top hat” fitting to the spectra results in <2 dB in expected RIN level, and the Gaussian was found to be closer to the measured data. For a spontaneous emission source, with Gaussian emission line shape, the white noise RIN level can be simplified to [29]

$$\frac{0.66}{\Delta\nu} \quad (1)$$

where the denominator is the bandwidth in Hertz. This dependence is plotted as a solid line in Fig. 6. An increase in bandwidth from 45 to 85 nm results in the observation of a 4 dB reduction in the noise background. Deviation from the predicted behavior of the ideal noise source may be attributed to the emission spectrum becoming increasingly non-Gaussian, tending towards a top hat shape with increasing bandwidth. For comparison, the RIN from the QW device at 1 mW output power is also plotted. The 2 dB lower RIN is attributed again to a difference in line shape, with the QW SLED giving a more Lorentzian emission. The bandwidth relationship of RIN for the three simple cases: top hat, Lorentzian, and Gaussian, respectively, are also plotted. Since the white noise level is dependent on both the source bandwidth and the emission spectrum, the spectral shaping as well as the bandwidth improvement should be considered [12].

In the TD OCT system used here, the typical detector bandwidth is ~ 100 kHz relating to 80 A-scans per second. In order to investigate the low-frequency behavior, a more detailed noise spectrum was obtained up to this frequency. A comparison of the QW and QD devices in this frequency range are shown in Fig. 7. The QD SLED demonstrates a lower noise at all frequencies increasing from 7.5 to 15 dB reduction at 100 kHz.

The white noise level in the SLED, determined by bandwidth, is therefore not the sole limit to the SNR of the emitted light. It is known that semiconductor amplifiers driven in the regime of gain saturation can increase SNR in optical networks [30], [31]. The light emitted by the SLED may be considered as a random spontaneous emission signal amplified in an SOA. By utilizing QDs, this noise reduction effect can be harnessed, since Pauli exclusion leads to state saturation, and in turn gain saturation, at

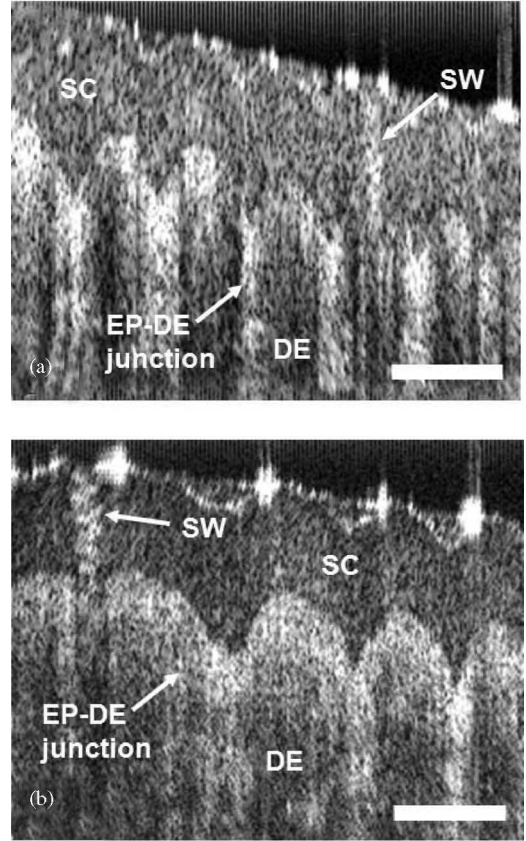


Fig. 8. *In vivo* skin images using (a) Superlum 561-MP and (b) QD SLED sources. Scale bar 500 μm .

relatively low carrier densities. It is the saturation effect that is also utilized in order to give the increased bandwidth by causing emission at the shorter wavelength excited state energies, in addition to that at the ground state. The result of this gain saturation is that the noise from the random spontaneous emission is not fully transferred to the amplified emission output. Therefore, RIN is reduced and the resulting system SNR is increased.

For a purely thermal source of Gaussian spectral width 85 nm, the SNR is 83 dB for a 100 kHz detector bandwidth [(from (1))]. However, the low-frequency-noise suppression observed in the QD SLED enables an increase of this SNR to 95 dB, obtained by integrating the data in Fig. 7. Significantly, this ~ 10 dB enhancement means the light source is no longer a limitation to system performance. Similar noise characteristics could be expected from QW SLED, if it were possible to achieve current densities high enough to utilize this gain saturation effects.

VI. IMAGING

Fig. 8 shows two OCT images of finger palmar skin, where the scale bar represents 500 μm . In both the cases, image contrast was enhanced by the application of glycerol to the skin.

Fig. 8(a) was obtained using the Superlum 561-MP QW-SLED, while Fig. 8(b) was obtained using the QD-SLED, described previously. The output powers (ex-fiber) of the devices are 1 mW and 10 mW for the QW and QD devices, respectively.

We reiterate that the comparison here is to highlight the effect of different output powers and bandwidth on OCT imaging, not the choice of active material. Both the images show epidermal and dermal structures, and have identical contrast settings.

Fig. 8(b), however, shows better resolution of the stratum corneum from lower layers of the epidermis. Similarly, there is stronger backscattering from the lower layers of epidermis and the sweat duct is better resolved in Fig. 8(b). This indicates the benefit of using high-power and higher bandwidth sources in OCT [32].

While depth penetration appears similar, investigating signals deeper than 1.1 mm shows better depth penetration for the higher power QD SLED (image not shown). The problem then becomes contrast, because the presence of signal does not always imply detection of an anatomical structure. It should be noted that safety requirements limit skin irradiation to about 10 mW [33], but this can be exceeded by pulsed sources for even better contrast and depth penetration. Fringe visibility is 7.7 dB higher using the 10 mW QD-SLED compared to the 1 mW commercial device. In theory, this value should scale with power (i.e., 10 dB). We are currently investigating the origin of the 2.3 dB discrepancy that is likely to be due to suboptimal alignment in the Fourier domain optical delay line of our TD OCT system.

VII. SUMMARY

We have presented a method for reducing the spectral dip usually associated with a QD active medium. By applying this active material in a multicontact SLED, we demonstrate ex-fiber powers of 18 mW and a bandwidth of 85 nm. We have shown how using a QD active operating under gain saturation allows emission broadening and brings about a reduction in RIN, and therefore, an improvement in SNR. Finally, we have shown, how an improvement in bandwidth, power, and noise translates into improved resolution and depth penetration by OCT *in vivo* imaging of skin by comparing to a commercial SLED.

REFERENCES

- [1] R. Ell, U. Morgner, F. X. Kärtner, J. G. Fujimoto, E. P. Ippen, V. Scheuer, G. Angelow, T. Tschudi, M. J. Lederer, A. Boiko, and B. Luther-Davies, "Generation of 5-fs pulses and octave-spanning spectra directly from a Ti: Sapphire laser," *Opt. Lett.*, vol. 26, pp. 373–375, Mar. 2001.
- [2] W. Drexler and J. G. Fujimoto, *Optical Coherence Tomography: Technology and Applications*. Berlin, Germany: Springer-Verlag, 2008.
- [3] J. F. de Boer, B. Cense, B. H. Park, M. C. Pierce, G. J. Tearney, and B. E. Bouma, "Improved signal-to-noise ratio in spectral-domain compared with time-domain optical coherence tomography," *Opt. Lett.*, vol. 28, no. 21, pp. 2067–2069, Nov. 2003.
- [4] R. Leitgeb, C. K. Hitzenberger, and A. F. Fercher, "Performance of Fourier domain vs. time domain optical coherence tomography," *Opt. Exp.*, vol. 11, no. 8, pp. 889–894, Apr. 2003.
- [5] R. Huber, D. C. Adler, and J. G. Fujimoto, "Buffered Fourier domain mode locking: unidirectional swept laser sources for optical coherence tomography imaging at 370000 lines/s," *Opt. Lett.*, vol. 31, pp. 2975–2977, Oct. 2006.
- [6] M. Wojtkowski, V. Srinivasan, T. Ko, J. Fujimoto, A. Kowalczyk, and J. Duker, "Ultrahigh-resolution, high-speed, Fourier domain optical coherence tomography and methods for dispersion compensation," *Opt. Exp.*, vol. 12, pp. 2404–2422, May 2004.
- [7] Y. Wang, J. S. Nelson, and Z. Chen, "Optimal wavelength for ultrahigh-resolution optical coherence tomography," *Opt. Exp.*, vol. 11, pp. 1411–1417, Jun. 2003.
- [8] J. Welzel, E. Lankenau, G. Hüttmann, and R. Birngruber, "OCT in dermatology," in *Optical Coherence Tomography*. Berlin, Germany/New York: Springer-Verlag, 2008, pp. 1103–1122.
- [9] L. H. Li, M. Rossetti, A. Fiore, L. Occhi, and C. Velez, "Wide emission spectrum from superluminescent diodes with chirped quantum dot multilayers," *Electron. Lett.*, vol. 41, no. 1, pp. 41–43, Jan. 2005.
- [10] S. K. Ray, T. L. Choi, K. M. Groom, H. Y. Liu, M. Hopkinson, and R. A. Hogg, "High-power 1.3- μm quantum-dot superluminescent light-emitting diode grown by molecular beam epitaxy," *IEEE Photon. Technol. Lett.*, vol. 19, no. 2, pp. 109–111, Jan. 2007.
- [11] S. K. Ray, T. L. Choi, K. M. Groom, B. Stevens, H. Liu, M. Hopkinson, and R. A. Hogg, "High-power and broad-band quantum dot superluminescent diodes centred at 1250 nm for optical coherence tomography," *IEEE J. Sel. Topics Quantum Electron.*, vol. 13, no. 5, pp. 1267–1272, Jun. 2007.
- [12] L. H. Li, M. Rossetti, and A. Fiore, "Chirped multiple InAs quantum dot structure for wide spectrum device applications," *J. Crystal Growth*, vol. 278, pp. 680–684, Jul. 2005.
- [13] P. D. L. Judson, K. M. Groom, D. T. D. Childs, M. Hopkinson, and R. A. Hogg, "Multi-section quantum dot superluminescent diodes for spectral shape engineering," *IET Optoelectron.*, vol. 3, pp. 100–104, Apr. 2009.
- [14] C. Ackay, P. Parrein, and J. P. Rolland, "Estimation of longitudinal resolution in optical coherence imaging," *Appl. Opt.*, vol. 41, no. 25, pp. 5256–5262, Aug. 2002.
- [15] S. K. Ray, K. M. Groom, H. Y. Liu, M. Hopkinson, and R. A. Hogg, "Broad-band superluminescent light emitting diodes incorporating quantum dots in compositionally modulated quantum wells," *Jpn. J. Appl. Phys.*, vol. 45, pp. 2542–2545, 2006.
- [16] G. T. Liu, A. Stintz, H. Li, T. C. Newell, A. L. Gray, P. M. Varangis, K. J. Malloy, and L. F. Lester, "The influence of quantum-well composition on the performance of quantum dot lasers using InAs/InGaAs dots-in-a-well (DWELL) structures," *IEEE J. Quantum Electron.*, vol. 36, no. 11, pp. 1272–1279, Nov. 2000.
- [17] H. Y. Liu, I. R. Sellers, D. J. Mowbray, M. S. Skolnick, K. M. Groom, M. Gutierrez, M. Hopkinson, J. S. Ng, J. P. R. David, and R. Beanland, "Improved performance of 1.3 μm multilayer InAs quantum-dot lasers using a high-growth-temperature GaAs spacer layer," *Appl. Phys. Lett.*, vol. 85, no. 5, pp. 704–706, Jun. 2004.
- [18] P. Blood, G. M. Lewis, P. M. Smowton, H. Summers, J. Thomson, and J. Lutti, "Characterisation of semiconductor laser gain media by the segmented contact method," *IEEE J. Sel. Topics Quantum Electron.*, vol. 9, no. 5, pp. 1275–1282, Oct. 2003.
- [19] X. L. Chu, M. Arzberger, G. Böhm, and G. Abstreiter, "Influence of growth conditions on the photoluminescence of self-assembled InAs/GaAs quantum dots," *J. Appl. Phys.*, vol. 85, p. 2355, Feb. 1999.
- [20] T. Ngo, P. M. Petroff, H. Sakaki, and J. L. Merz, "Simulation model for self-ordering of strained islands in molecular beam epitaxy," *Phys. Rev. Online*, vol. B53, pp. 9618–9621, Feb. 1996.
- [21] S. J. Leea, S. K. Noh, J. W. Choe, and E. K. Kim, "Evolution of bimodal size-distribution on InAs coverage variation in as-grown InAs/GaAs quantum-dot heterostructures," *J. Crystal Growth*, vol. 267, pp. 405–411, Dec. 2004.
- [22] D. Bimberg, "Onion like growth and inverted many-particle energies in quantum dots," *Appl. Surface Sci.*, vol. 255, pp. 799–801, Sep. 2008.
- [23] Y. Xin, A. Martinez, T. A. Nilsen, A. Moscho, Y. Li, A. L. Gray, and L. F. Lester, "1.3 μm quantum dot multi-section superluminescent diode with extremely broad bandwidth ($>150\text{ nm}$)," *IEEE Photon. Technol. Lett.*, vol. 19, no. 7, pp. 501–503, Apr. 2007.
- [24] P. D. L. Greenwood, D. T. D. Childs, K. M. Groom, B. J. Stevens, M. Hopkinson, and R. A. Hogg, "Tuning superluminescent diode characteristics for optical coherence tomography systems by utilising a multi-contact device incorporating wavelength modulated quantum dots," *IEEE J. Sel. Topics Quantum Electron.*, vol. 15, no. 3, pp. 757–763, May 2009.
- [25] V. R. Shidlovski, "SLD Sensitivity to Optical Feedback," Superlum Diodes Ltd., Moscow, Russia, Appl. Note, 2006.
- [26] I. Middlemast, J. Sarma, and S. Yunus, "High power tapered superluminescent diodes using novel etched deflectors," *Electron. Lett.*, vol. 33, no. 10, pp. 903–904, Mar. 1997.
- [27] P. D. L. Greenwood, K. V. Patel, D. T. D. Childs, K. M. Groom, B. J. Stevens, M. Hopkinson, and R. A. Hogg, "Multi-contact quantum dot superluminescent diodes for optical coherence tomography," *SPIE Proc.*, vol. 7230, pp. 72300C-1–72300C-10, Feb. 2009.
- [28] N. Krstajić, L. E. Smith, S. J. Matcher, D. T. D. Childs, M. Bonesi, P. D. L. Greenwood, M. Hugues, K. Kennedy, M. Hopkinson, K. M. Groom, S. MacNeil, R. A. Hogg, and R. Smallwood, "Quantum dot superluminescent diodes for optical coherence tomography: Skin imaging," *IEEE*

- J. Sel. Topics Quantum Electron.*, vol. 16, no. 4, Jul./Aug. 2010, to be published.
- [29] M. Tur, E. Shafir, and K. Blotek, "Source induced noise in optical systems driven by low coherence sources," *J. Lightw. Technol.*, vol. 8, pp. 183–189, Feb. 1990.
- [30] M. Shtaif and G. Eisenstein, "Noise properties of nonlinear semiconductor optical amplifiers," *Opt. Lett.*, vol. 21, pp. 1851–1853, Nov. 1996.
- [31] A. D. McCoy, P. Horak, B. C. Thomsen, M. Ibsen, and D. J. Richardson, "Noise suppression of incoherent light using a gain saturated SOA: Implications for spectrum sliced WDM systems," *J. Lightw. Technol.*, vol. 23, pp. 2399–2409, Aug. 2005.
- [32] W. Drexler, "Ultrahigh-resolution optical coherence tomography," *J. Biomed. Opt.*, vol. 9, pp. 47–74, Jan./Feb. 2004.
- [33] P. International Commission on Non-Ionizing Radiation, "ICNRP statement on light-emitting diodes (LEDs) and laser diodes: Implications for hazard assessment," *Health Phys.*, vol. 78, pp. 744–752, Oct. 2000.



Purnima D. L. Greenwood (nee Judson) was born in 1984. She received the B.Sc. (Hons.) degree in physics from Dundee University, Dundee, U.K., in 2004. She is currently working toward the Ph.D. degree in electronic and electrical engineering, University of Sheffield, Sheffield, U.K. Her research has been concerned with quantum dot superluminescent diodes for imaging using optical coherence tomography.



David T. D. Childs received the B.Sc. degree in physics and the M.Sc. degree in semiconductor science and technology, and the Ph.D. degree from Imperial College London, London, U.K., in 1996, 1997, and 2002, respectively.

He was with the R&D Department of Bookham (formerly Marconi Optical Components) at the Caswell Semiconductor Research and Fabrication Facility until 2006, where he was involved in many aspects of the design and characterization of improved active and tuning regions for DFB and multi-section

tunable distributed Bragg reflector laser devices. He is currently with the Department of Electronic and Electrical Engineering, the University of Sheffield, Sheffield, U.K., where he is engaged in quantum dot devices for application in optical communications and biomedical imaging.



Kenneth Kennedy received the B.Sc. (Hons.) degree in optoelectronics and laser engineering from Heriot-Watt University, Edinburgh, U.K., in 1999. Since 2004, he has been working toward the Ph.D. degree in quantum cascade distributed feedback lasers with the Department of Electronic and Electrical Engineering, University of Sheffield, Sheffield, U.K.

He was with Hewlett-Packard, Ipswich, U.K., as a Manufacturing Engineer, where he was engaged in telecom wavelength semiconductor lasers and detectors. During 2003, he was a Technology Transfer

Engineer with Agilent Technologies Ltd, Singapore. Since August 2008, he has been a Research Associate at the University of Sheffield, where he is engaged in compound semiconductor emitters.



Kristian M. Groom received the M.Phys. and Ph.D. degrees from the University of Sheffield, Sheffield, U.K., in 1999 and 2003, respectively.

He is currently with the Department of Electronic and Electrical Engineering, University of Sheffield. He was involved in long wavelength GaAs-based lasers and superluminescent diodes such as those based on quantum dots. He is the author or coauthor of over more than 40 papers published in various international journals and conference proceedings.

Dr. Groom was a recipient of the Royal Academy of Engineering/Engineering and Physical Sciences Research Council Fellowship Award in 2005 for research into advanced semiconductor laser engineering.

Maxime Hugues received the M.Sc. degree in material and device physics from Joseph Fourier University, Grenoble, France, in 2004 and the Ph.D. degree in applied physics from Nice Sophia Antipolis University, Nice, France, in 2007.

He was with the Centre de Recherche sur l'Hétéroépitaxie et ses Applications-Centre National de la Recherche Scientifique, Valbonne, Sophia Antipolis, France, where he was engaged in dilute nitride and InAs quantum dots for long-wavelength GaAs based lasers. He is currently with the Department of Electronic and Electrical Engineering, University of Sheffield, Sheffield, U.K., where he is engaged in the III-V nanostructures growth by molecular beam epitaxy at the Engineering and Physical Sciences Research Council National Centre for III-V Technologies.



Mark Hopkinson received the B.Sc. from the University of Birmingham, Birmingham, U.K., in 1986 and the Ph.D. degree in hydrogenated amorphous silicon from the University of Sheffield, Sheffield, U.K., in 1990.

He was a Postdoctoral Researcher at the University of Warwick, Coventry, U.K. and the University of Sheffield, and a Senior Process Engineer at Marconi PLC. Since 2002, he has been a Leader of the Research Group involved in the development of III-V epitaxial nanostructures by molecular beam epitaxy,

with emphasis on novel optoelectronic devices at the Department of Electronic and Electrical Engineering, University of Sheffield. He has 17 years experience in the field of Electronic Engineering. He is the author or coauthor of over more than 450 papers published in various international journals and conference proceedings. His research interests include III-V quantum dot materials and novel quantum well systems, including antimonide-based structures and dilute nitride materials.

Dr. Hopkinson was awarded a Chair in Electronic Engineering in 2007.



Richard A. Hogg received the Ph.D. degree from the University of Sheffield, Sheffield, U.K., in 1995.

He was a Postdoctoral Researcher at Nippon Telegraph & Telephone Corporation Basic research Laboratories, Atsugi, Japan for two years. He subsequently spent the next three years at Toshiba Research Europe's Cambridge Laboratory, before moving to Agilent Technologies Fibre-Optic Component Operation in 2000. Since 2003 he has been with the Electronic and Electrical Engineering Department, University of Sheffield. His research group has been engaged in the

development of quantum dot lasers and superluminescent diodes, and quantum cascade DFBs.

Dr. Hogg was a recipient of an EU-Japan Fellowship Award as a Visiting Researcher in Professor Arakawa's Laboratory, University of Tokyo.

Nikola Krstajić was born in Belgrade, Serbia, in 1973. He received the M.Eng. degree in electronics from the University of Salford, Manchester, U.K., in 1997 and the Ph.D. degree in physics from the University of Surrey, Guildford, U.K., in 2007.

During 1997 to 2003, he was with medical and scientific instrumentation companies including Oxford Instruments and Melles Griot. Currently he is a Research Associate in biophotonics with the Department of Computer Science, University of Sheffield.

Louise E. Smith received the B.Eng. (Hons.) degree in biomedical materials science and engineering from the Queen Mary, University of London, London, U.K., in 2003 and the Ph.D. degree in the development of poly(vinylpyrrolidinone) networks for treatment of skin graft contracture from the University of Sheffield, Sheffield, U.K., in 2008.

She is currently a Postdoctoral Research Associate in tissue engineering at the University of Sheffield. Her current research has been concerned with non-invasively monitoring cell migration within tissue-engineered skin constructs including construct maturation.

Stephen J. Matcher received the B.Sc. degree in physics and the Ph.D. degree in optical astronomy from Imperial College London, London, U.K., in 1985 and 1989, respectively.

In 1992, he joined the Biophotonics Group at University College London, London, U.K., where he was engaged in near-infrared spectroscopy of tissues. In 1996, he joined the the Physics Department, University of Exeter, Exeter, Devon, U.K., where he developed Doppler and polarization-sensitive optical coherence tomography techniques. Since 2006, he joined the Department of Engineering Materials, at University of Sheffield, Sheffield, U.K. His current research interest includes OCT imaging in tissue engineering and regenerative medicine.

Marco Bonesi received the Graduate degree in electronic engineering, bioengineering (M.S. equivalent), from the University of Trieste, Trieste, Italy, in 2002, and the Ph.D. degree in biomedical optics from Cranfield University, Cranfield, U.K., in 2008.

He is currently a Postdoctoral Research Associate of Biomedical Optics at the Medical University of Vienna, Vienna, Austria, where he was involved in the studies of application of optical techniques for fluid dynamics characterization in microcirculation and biological tissues investigations.

Sheila MacNeil received the B.Sc. (Hons.) degree in physiology from Aberdeen University, Aberdeen, U.K., in 1972 and the Ph.D. degree in physiology from the University of Sheffield, Sheffield, U.K., in 1976.

She was a Postdoctoral Fellow with the Royal Hallamshire, and also a Postdoctoral Fellow at Northern General Hospitals, Sheffield, where she was appointed a Wellcome Trust Funded Lecturer in the Department of Clinical Sciences, in 1986. Since 2000, she has been a Professor of tissue engineering with The University of Sheffield, where she currently leads a large multidisciplinary group, based in the Kroto Research Institute. Her current research interests include soft tissue engineering and biomaterials. She has been associated with clinical colleagues in the National Health Service in Burns and Plastics and in Dermatology and with academic colleagues in Chemistry and Engineering Materials and Computational Biology.

Rod Smallwood received the Ph.D. degree in medical physics from the University of Sheffield, Sheffield, U.K., in 1976.

He is currently a Professor of computational biology at the University of Sheffield with a joint appointment in the Department of Computer Science and the Medical School, the University of Sheffield.

Dr. Smallwood is a Fellow of the Royal Academy of Engineering.